The Application of Four-Wave Mixing to Cold and Ultra-Cold Atom Imaging

Francesca Fornasini

May 11, 2010

Advisors: Seth Aubin and Irina Novikova

Abstract

In this project, I investigated a new imaging technique for cold and ultra-cold atoms based on the four-wave mixing (FWM) process. In theory, this technique will provide more precise measurements of the number and spatial density distribution of cold atoms than fluorescence or absorption imaging. Since FWM is usually studied in high optical depth vapor cells but cold atoms have low optical depths, I first studied the dependence of FWM on optical depth. Results showed that Stokes field emission due to FWM decreases exponentially with decreasing optical depth, and that it can still be observed at optical depths of ≈1. After determining the optimal conditions for Stokes field emission, I tried observing FWM with cold atoms. Absorption and emission-like features were observed on the probe and Stokes fields which depended on the interaction of the control field, the probe field, and the trapped atoms. There is significant reason to believe that these features are associated with the FWM process, although further studies need to be undertaken to determine more definitively the nature of these features, how they depend on various parameters of the experimental setup, and how they may be related to the number and density of the cold atoms.

1 Introduction

When atoms approach a phase-space density of 1, corresponding to temperatures around or below tens of microKelvin, they enter the quantum regime and behave quite differently than they do in the classical regime. The resulting quantum gases of fermions or bosons are interesting to study in and of themselves. Ultra-cold bosons, such as ^{87}Rb, all occupy the same motional ground state of the system, forming Bose-Einstein condensates. Ultra-cold fermions, such as ^{40}K, cannot all occupy the ground state due to the Pauli exclusion principle; instead, they fill up the energy levels of the system starting from the ground state up

to a maximum energy level determined by the number of particles. Gases of ultra-cold fermions are called degenerate Fermi gases. Because of these properties, ultra-cold atoms can also be used to make precision measurements of accelerations, rotations, the magnetic and electric dipole moments of atoms and molecules, and weak forces in the vicinity of surfaces, such as submillimeter gravity and the Casimir-Pölder force.

Having an imaging system which can accurately measure the number and spatial distribution of ultra-cold atoms is very important for ultra-cold atom research. Currently, the two most common techniques for imaging atoms only work well for low densities or for very large numbers of atoms, while ultra-cold condensates have high densities and, oftentimes, small numbers of atoms. The first of these techniques, fluorescence imaging, consists in exciting the atoms with laser light tuned to a resonant transition frequency and capturing the spontaneously emitted photons with a charge-coupled device (CCD). While having the advantage of providing images with zero background, this method only provides an accurate measurement of the number of atoms in a low density system, because otherwise a photon re-emitted by one atom may easily be absorbed by another; furthermore, only a fraction of the emitted photons can be collected since they scatter in all directions. The second technique, absorption imaging, involves shining a beam of light with a large diameter and a resonant frequency on the atomic cloud and imaging its shadow; this method only yields reliable results for large numbers of atoms due to the significant background signal.

This thesis describes a potentially more effective method for imaging cold and ultra-cold atoms based on four-wave mixing (FWM), a nonlinear process in which the simultaneous interaction of atoms with two near-resonant laser fields leads to the generation of a third coherent field.

Section 1.1 discusses four-wave mixing and its advantages in greater detail. Sections 2-4 describe the study of FWM in different experimental setups. Since FWM is usually studied at high optical depths of $\approx$50-70 while ultra-cold atoms have low optical depths of $\approx$1, it was first necessary to determine whether FWM was observable at low optical depths, where optical depth (OD) is defined by:

$$\frac{I_{OUT}}{I_{IN}} = e^{-OD} \tag{1}$$

Thus, as discussed in section 2, the dependence of FWM on optical depth was observed in an already-existing vapor cell setup in which the three FWM beams were colinear. Then, as dicussed in section 3, a setup more useful for imaging purposes was developed; in this setup, the three beams were non-colinear, but a vapor cell was still used. The vapor cell was initially at a high optical depth in order to maximize the FWM signals, making it easier to test the setup and optimize the FWM process. Once optimal conditions were determined, the optical depth of the vapor cell was lowered in order to observe the dependence of FWM on optical depth. Finally, as described in section 4, several changes were made to this second setup in order to use it with cold atoms. This section also discusses the exciting and promising observation of cold atom-laser interaction signals consistent with FWM.

1.1 Four-Wave Mixing

Four-wave mixing is a nonlinear, two-photon process which involves the interaction of atoms with two laser beams of different near-resonant frequencies and results in the emission of photons with a third, off-resonant frequency. The basic schematic of this process is shown in Figure 1. The two beams directed onto
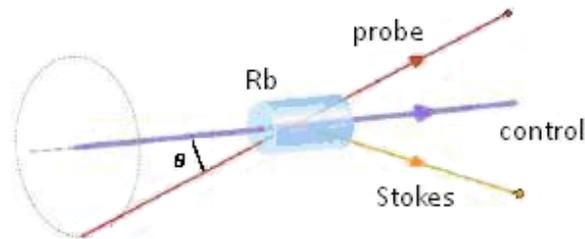
Figure 1: Schematic of four-wave mixing in Rb cell (adapted from [1])

the atoms are referred to as the control, or pump, beam and the probe beam. In some recent experiments, the probe beam has a much lower intensity than the control beam; recent literature indicates that the control beam is generally in the hundreds of mW range, while the probe beam is in the hundreds of μW range [2, 3]. Furthermore, the control and the probe beams are oriented at a small angle θ with respect to each other, which is usually around 0.2°-0.5° [2, 3, 4]; since the angle is small, the control and probe fields almost completely overlap as they pass through the Rb vapor cell. When FWM occurs due to a nonlinear optical process, the control beam passes through the atoms relatively unaffected, the probe beam is amplified or attenuated, and a third beam called the Stokes, or conjugate, beam is emitted by the system.

1.1.1 Nonlinear Induced Polarization

The theoretical model describing the FWM process has been carefully developed by recent studies [5], so it is only discussed briefly here. The induced polarization of an electric field passing through a cell of atoms is nonlinear and significant up to third order in the electric susceptibility:

$$\frac{P_i}{\epsilon_0} = \sum \chi_{ij}^{(1)} E_j + \sum \chi_{ijk}^{(2)} E_j E_k + \sum \chi_{ijkl}^{(3)} E_j E_k E_l \tag{2}$$

The total electric field consists of the sum of the control and probe fields, such that

$$\mathbf{E} = E_{0_c} \cos(\mathbf{k}_c \cdot \mathbf{r} - w_c t) + E_{0_p} \cos(\mathbf{k}_p \cdot \mathbf{r} - w_p t) \tag{3}$$

where the subscript c refers to the control field, and the subscript p refers to the probe field. The interaction of this composite electric field with the third order term of the induced polarization (i.e. $\chi^{(3)} \mathbf{E}^{(3)}$), plus the restrictions imposed by conservation of energy and momentum yield the creation of a field propagating in

the direction $\mathbf{k}_s{=}2\mathbf{k}_c{-}\mathbf{k}_p$ with frequency $\omega_s{=}2\omega_c{-}\omega_p$. It can be shown that a term with this form appears when the electric field is cubed as part of Equation 2. Substituting φ_c for $\mathbf{k}_c \cdot \mathbf{r} - w_c t$ and φ_p for $\mathbf{k}_p \cdot \mathbf{r} - w_p t$, Equation 4 raised to the third power is equal to:

$$\left[E_{0_c}\cos\varphi_c + E_{0_p}\cos\varphi_p\right]^3 = E_{0_c}^3\cos^3\varphi_c + E_{0_p}^3\cos^3\varphi_p + 3E_{0_c}^2 E_{0_p}\cos^2\varphi_c\cos\varphi_p + 3E_{0_c}E_{0_p}^2\cos\varphi_c\cos^2\varphi_p \quad (4)$$

The first two terms correspond to the generation of the third harmonic of each field; the last two terms correspond to FWM. Applying some trigonometric identities to the first FWM term yields:

$$
\begin{aligned}
E_{0_c}^2 E_{0_p}\cos^2\varphi_c\cos\varphi_p &= \frac{1}{2}E_{0_c}^2 E_{0_p}\left(1 + \cos(2\varphi_c)\right)\cos\varphi_p \\
&= \frac{1}{2}E_{0_c}^2 E_{0_p}\cos\varphi_p + \frac{1}{4}E_{0_c}^2 E_{0_p}\left[\cos(2\varphi_c + \varphi_p) + \cos(2\varphi_c - \varphi_p)\right] \quad (5)
\end{aligned}
$$

Substituting in the original values of φ_c and φ_p into the final term of Equation 5 gives:

$$\frac{1}{4}E_{0_c}^2 E_{0_p}\cos(2\varphi_c - \varphi_p) = \frac{1}{4}E_{0_c}^2 E_{0_p}\cos\left[(2\mathbf{k}_c - \mathbf{k}_p)\cdot\mathbf{r} - (2w_c - w_p)t\right] \quad (6)$$

The frequency $2\omega_c{-}\omega_p$ is the frequency of the Stokes field (which is explained with reference to atomic transitions in Figure 3). The k-vector $2\mathbf{k}_c{-}\mathbf{k}_p$ defines the direction of propagation of the Stokes field; since $\mathbf{k}_c$ and $\mathbf{k}_p$ are at a small angle θ with respect to each other, the direction of the Stokes signal will be at an angle of approximately $-\theta$ with respect to the control field.

Although this nonlinear effect always occurs, the amplitude of the term corresponding to the Stokes signal depends on the detuning of the control and probe lasers from the resonance transitions of the atoms. This amplitude, and therefore the Stokes signal, is greatest when the two-photon resonance condition is satisfied and both lasers have frequencies that are close to atomic transition frequencies. Before explaining how the two-photon condition can be met, it is necessary to be familiar with the energy levels of ^{87}Rb, the atom used in this experiment.

1.1.2 ^{87}Rb Energy Levels

Rubidium, like hydrogen and the alkali metals, has one outermost valence electron, which is the only one involved in the atomic transitions of FWM. The ground state of this electron is the $5S_{1/2}$ state; its first two excited states are the $5P_{1/2}$ and $5P_{3/2}$ states, which are fine-split due to their total angular momentum J values. The D1 line refers to the transitions between the $5S_{1/2}$ and the $5P_{1/2}$ state; the D2 line refers to the transitions between the $5S_{1/2}$ and the $5P_{3/2}$ state. The ^{87}Rb nucleus has a nuclear spin of I = 3/2; the interaction of the nuclear spin I and the angular momentum J causes hyperfine splitting of both the S and P levels, as shown in Figure 2.
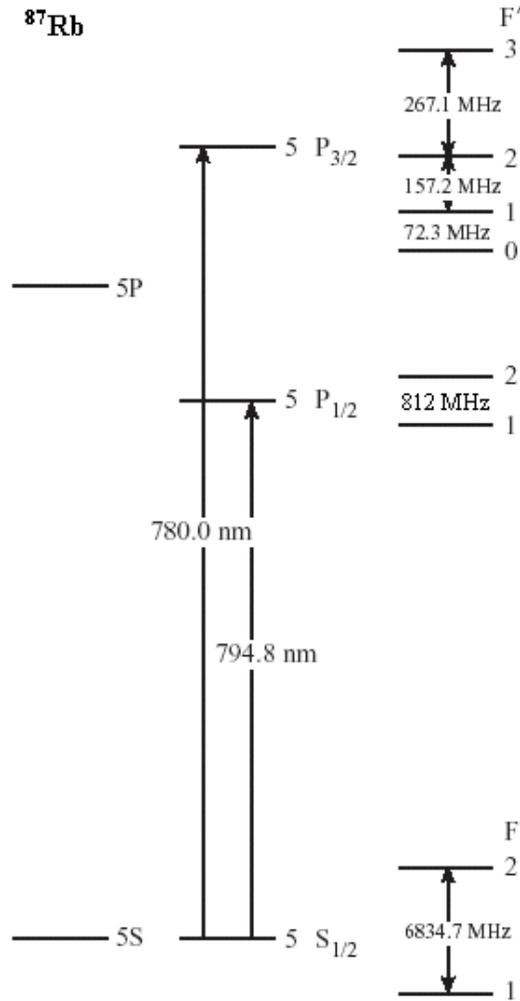
Figure 2: [87]Rb D1 line and D2 line energy levels (adapted from [6])

1.1.3 Two-Photon Resonance

Figure 3 illustrates how the control and probe lasers must be tuned in order for FWM to occur when using the D1 line transitions of [87]Rb. The control field is slightly detuned from the F=1→F'=2 transition, while the probe field is detuned by the same amount from the F'=2→F=2 transition. It is crucial that the frequency difference between the control and probe fields be equal to the frequency difference between the two ground states; this is what is known as the two-photon resonance condition. The Stokes field is emitted as a result of the control field acting on the F=2 rather than the F=1 state.

This generated Stokes field, which depends on the number of atoms with which the control and probe fields interact, can be used to image ultra-cold atomic clouds, and it should provide an accurate measurement of even small numbers of atoms at high density. FWM should eliminate some of the problems inherent in
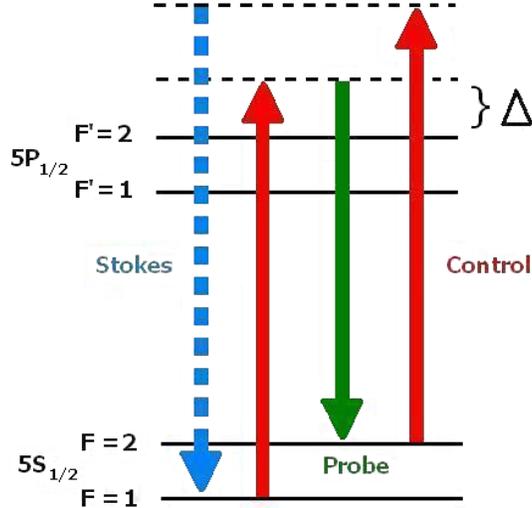
Figure 3: Energy level diagram for four-wave mixing in ^{87}Rb. Δ is laser detuning from resonance.

fluorescence and absorption imaging. It should provide signals with zero background so that even signals due to small numbers of atoms can be detected. Furthermore, since the Stokes photons are emitted in a single and predictable direction, all the photons, not just a fraction of them, can be collected. Finally, since the emitted photons are off-resonant with the transition frequencies of the atoms, they should not be re-absorbed by the other atoms they encounter in the high density environments of ultra-cold atoms.

2   FWM in Colinear Setup

Before trying to observe FWM in cold atoms, I studied the FWM process in one of Novikova's already-functioning experimental setups involving a Rb vapor cell (see [7]). FWM is usually studied in vapor cells at optical depths of 50-70, but cold atoms have optical depths of $\approx$ 1. Thus, before devising a new setup for imaging purposes or trying to observe FWM in cold atoms, it was necessary to study the FWM process as a function of optical depth and to determine whether it is observable at low optical depths.

2.1   Experimental Setup

In the original experimental arrangement, the control, probe, and Stokes fields all originated from a single laser beam and perfectly overlapped as they propagated through a Rb vapor cell. This colinear experimental setup is shown in Figure 4. In this schematic, the optical elements that simply serve to change the beam sizes and shapes as well as the reference cells used to tune each laser to the ^{87}Rb transitions have been

omitted. A single diode laser (DL100 from Toptica) was detuned slightly to the blue of the F=2→F'=2 transition. After the beam passed through the acousto-optic modulator (AOM), the first-order diffraction peak, whose frequency was lowered by 80 MHz with respect to the zeroeth-order, was selected and sent to the electro-optic modulator (EOM). By phase-modulating the laser beam, the EOM created two frequency sidebands, one that was 6.8 GHz higher than the control field frequency and one that was 6.8 GHz lower than the control field frequency. The field with the higher frequency was the Stokes field while the field with the lower frequency was the probe field, which in this setup was being sent into the ^{87}Rb cell with the other fields. The power of the EOM controlled the relative powers of the three fields. Before entering the Rb cell, all three fields were circularly polarized. The Rb vapor cell was 25.5 mm long, contained a Neon buffer, was encased in magnetic shielding, and was equipped with a temperature controller. In order to detect the three light fields present within the single beam leaving the Rb cell, this beam was recombined with a fraction of the original laser beam which had not passed through the AOM; since the AOM introduced a 80 MHz frequency shift to the beam, recombining the two beams created beat notes differentiating the Stokes and probe fields. This recombined beam was then sent to a fast photodiode and a spectrum analyzer.
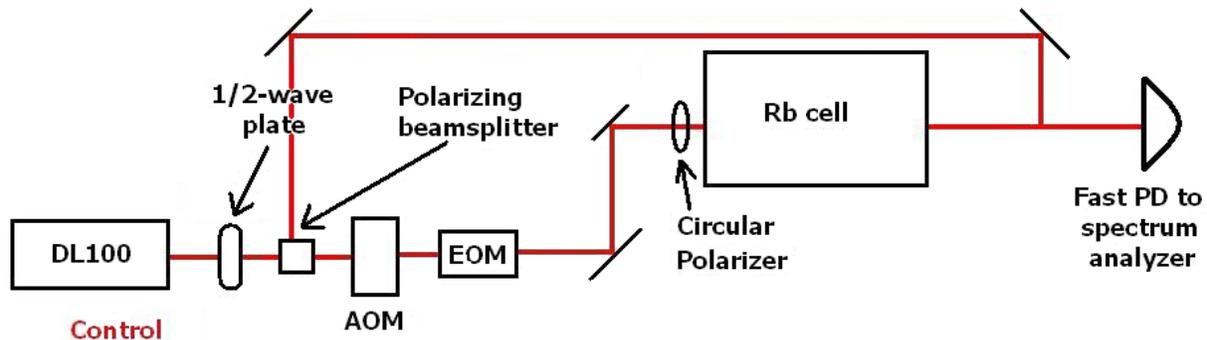
Figure 4: Schematic of colinear setup

2.2 Data and Analysis

2.2.1 Probe and Stokes dependence on optical depth

The probe and Stokes signals were measured at six different temperatures, corresponding to optical depths of 18, 14, 10, 6, 3, and 1. The purpose of these measurements was to assess the dependence of FWM on optical depth and to determine whether it is still observable at low optical depths comparable to those of ultra-cold atoms (0.5<OD<1.5). At each of these six optical depths, I measured the probe and Stokes signals for different values of the total laser power within a range of 0.9 mW to 4.5 mW. As the optical

depth decreased, the signals became weaker but continued to be visible, especially by time-averaging them on the spectrum analyzer. Since these signals had significant backgrounds, I also measured the background of each signal by tuning the EOM frequency sidebands away from the two-photon resonance condition and recording the resulting signal, which showed no signs of FWM.
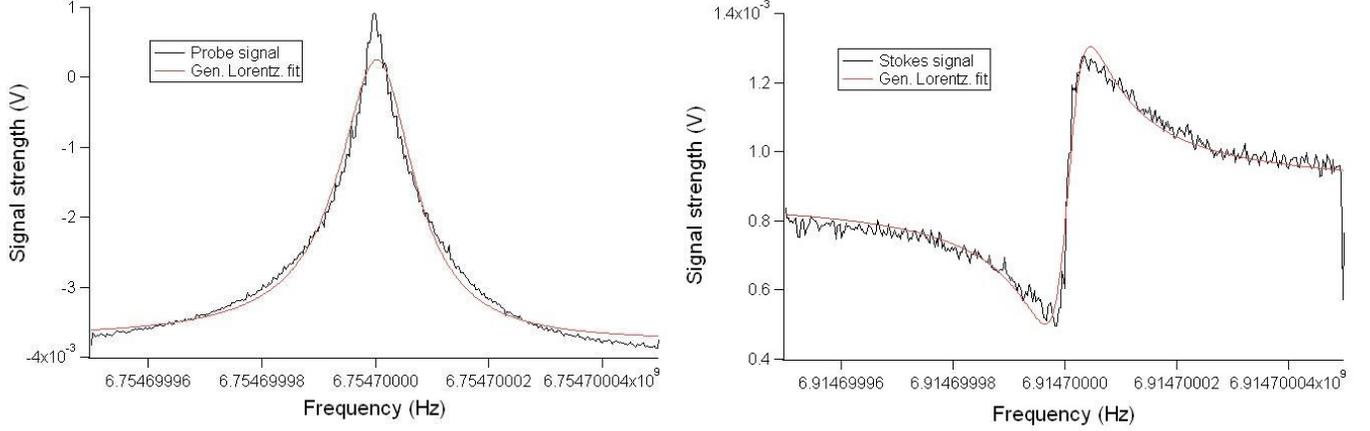
Figure 5: Probe and Stokes signals at $\tau = 14$, laser power $= 0.9$ mW

I used the Igor Pro analysis software to analyze the data. I subtracted the background levels from both the Stokes and probe measurements, which not only set the "background" of these signals at zero, but also helped correct for the curvature due to the spectrum analyzer bandwidth limit on frequency scans. Then I fit a generalized Lorentzian function of the form shown in Equation 7 to all the signals:

$$L(x) = \frac{A\gamma + B(x - x_0)}{\gamma^2 + (x - x_0)^2} \tag{7}$$

where x is the frequency difference between the control field and the probe or Stokes field. I examined the fits to ensure that they were appropriate. The probe signal consisted of a transmission peak which was mostly symmetric (the A coefficient dominated), whereas the Stokes signal was an antisymmetric combination of an absorption and an emission peak (the B coefficient dominated). Figure 5 provides examples of the probe and Stokes signals with their Lorentzian fits; although the fits are not ideal because the resonance peaks are much sharper than Lorentzian functions, they still provide a fairly accurate and easy way of gauging the relative heights of the peaks. Figure 6 and Figure 7 illustrate how these coefficients change as a function of optical depth. The data recorded at OD $= 18$ was omitted from these plots, because these first measurements contained a lot of human error. In each plot, coefficients are plotted for three different values of the laser power to demonstrate that similar trends occur at all laser powers, and that as laser power decreases, the coefficients and, therefore, the strength of the FWM peaks tends to decrease. The fits shown on these plots

8

were estimated manually by assuming they had the form:

$$y = ae^{bx} + x_0 \tag{8}$$

I adjusted the parameters a, b, and x_0 until I found a good fit. All the fits have similar parameters, as shown in Equation 9 to Equation 14. Thus, both the Stokes and probe FWM peaks tend to exponentially decrease in the same way as optical depth decreases.

$$\text{ProbeACoeff} = 8 \times 10^{-5} e^{0.26 \times OD} - 5 \times 10^{-5}, \text{power} = 4.5\text{mW} \tag{9}$$

$$\text{ProbeACoeff} = 8 \times 10^{-5} e^{0.26 \times OD} + 1 \times 10^{-5}, \text{power} = 2.7\text{mW} \tag{10}$$

$$\text{ProbeACoeff} = 9 \times 10^{-5} e^{0.27 \times OD} - 5 \times 10^{-5}, \text{power} = 0.9\text{mW} \tag{11}$$

$$\text{StokesBCoeff} = 9 \times 10^{-5} e^{0.32 \times OD} - 2 \times 10^{-5}, \text{power} = 4.5\text{mW} \tag{12}$$

$$\text{StokesBCoeff} = 5 \times 10^{-5} e^{0.33 \times OD} - 5 \times 10^{-5}, \text{power} = 2.7\text{mW} \tag{13}$$

$$\text{StokesBCoeff} = 4 \times 10^{-5} e^{0.28 \times OD} - 2 \times 10^{-5}, \text{power} = 0.9\text{mW} \tag{14}$$
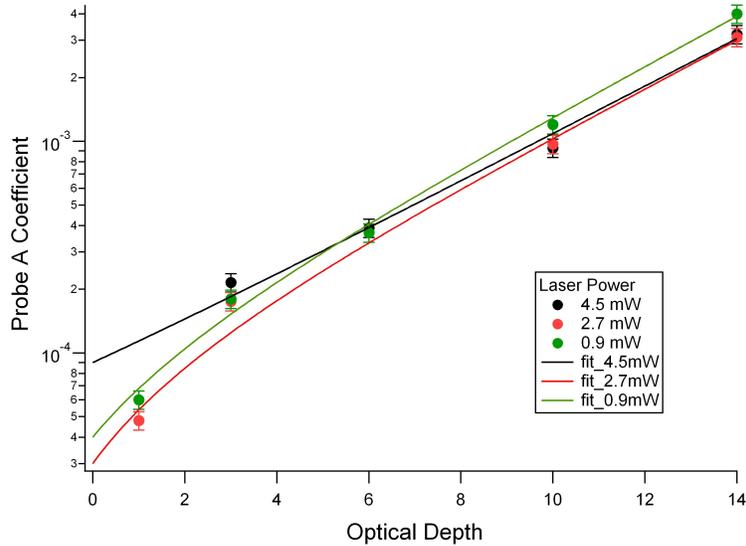
Figure 6: Plot of probe A coefficient vs. optical depth. The A coefficient fits have a $\pm 10\%$ error.

At an optical depth of 1.0, the Stokes signal had to be averaged for 30-60 seconds to achieve signal-to-noise ratios of approximately 2, but it was observable even without averaging. Furthermore, the fits predict it should still be detectable at an optical depth of 0.5. Since the optical depths of ultra-cold atoms are typically between 0.5 and 1.5, these results indicate that FWM should be observable in cold and ultra-cold atoms, although it would be helpful to find ways of optimizing Stokes emission and increasing the signal-to-noise ratio.

9
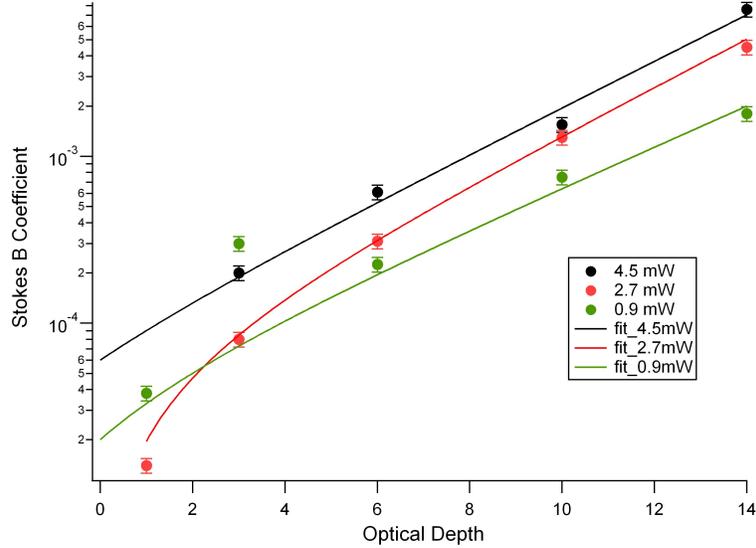
Figure 7: Plot of Stokes B coefficient vs. optical depth. The B coefficient fits have a $\pm 10\%$ error.

3   FWM in Non-colinear Setup

Although the colinear setup was used to study the dependence of FWM on optical depth, this setup was not suitable for the intended FWM imaging application, which is why a new setup was constructed in which the control and probe fields are not colinear. This non-colinear setup can theoretically yield zero background Stokes signals, and it allows the Stokes and probe fields to be easily separated due to the small angle between them. The same heated Rb vapor cell was used to study how Stokes field emission could be optimized and to measure the dependence of the Stokes signal on optical depth in this new setup.

3.1   Experimental Setup

The basic experimental setup is shown in Figure 8. The control and probe fields were provided by two different diode lasers which were not phase locked; both beams were linearly polarized and orthogonal to each other, as recommended by [8]. The beams entered the ^{87}Rb vapor cell at a small angle θ relative to one another. The intensity of each field could be controlled by adjusting the polarization direction of the half-wave plate preceding their respective beamsplitters, and also, in the case of the control field, by adjusting the power supplied to the AOM. After the Rb cell, a polarizer blocked the control field, but let the probe and Stokes fields, which have the same polarization, pass through; in practice, the control field was not completely blocked and showed up as background on the Stokes signal. Furthermore, since θ was approximately $0.2°$ and the beams were still very close together at the end of the table, an edge mirror was used to separate the probe and Stokes fields after the polarizer, but they could never be perfectly separated. Finally, the probe

and Stokes fields were detected by two different photodiodes (PD) connected to an oscilloscope. It should be noted that a 10 kΩ resistor was connected to the probe photodiode while a 390 kΩ resistor was connected to the Stokes photodiode, because the Stokes current was much smaller than the probe current.
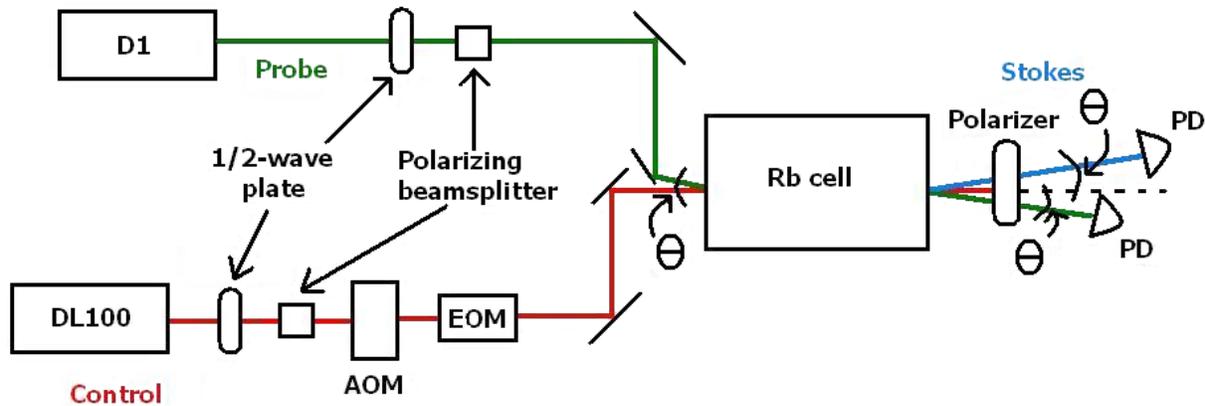
Figure 8: Basic experimental setup

3.2   Data and Analysis

3.2.1   Finding the Stokes signal

In order to be able to easily detect and optimize the Stokes signal during the initial measurements, the optical depth of the cell was set to ≈70. To search for signs of FWM, the DL100 laser was tuned to a frequency 500-800 MHz greater than the F=1→F'=2 ^{87}Rb transition frequency, because this is a typical laser detuning value [8]. The D1 laser was scanned across a large range of frequencies centered around the F=2→F'=2 transition. Figure 9 displays the absorption spectra of ^{87}Rb and ^{85}Rb, which could be seen on an oscilloscope by means of a Rb reference cell and then used to tune the lasers to the desired frequencies. After adjusting various parameters such as laser powers and frequency detunings, a sharp spike appeared on the probe signal at one particular frequency, which was an indication that the control and probe fields were interacting at this particular probe frequency. Narrowing the frequency scan so as to be centered more closely on this probe FWM resonance, I then searched for the Stokes signal with both a photodiode and a camera at the angle where it was theoretically predicted to be.

Eventually, I found the Stokes beam, which was too faint to be seen using infrared sensitive cards. I performed several "tests" to confirm that the signal I found with the photodiode was really the Stokes field. This signal was positioned on the opposite side of the control beam with respect to the probe beam. Furthermore, it had the same polarization as the probe, it disappeared if either the control or the probe beam was blocked, and, on the camera, it flashed proportionately to the speed of the probe frequency scan.

11
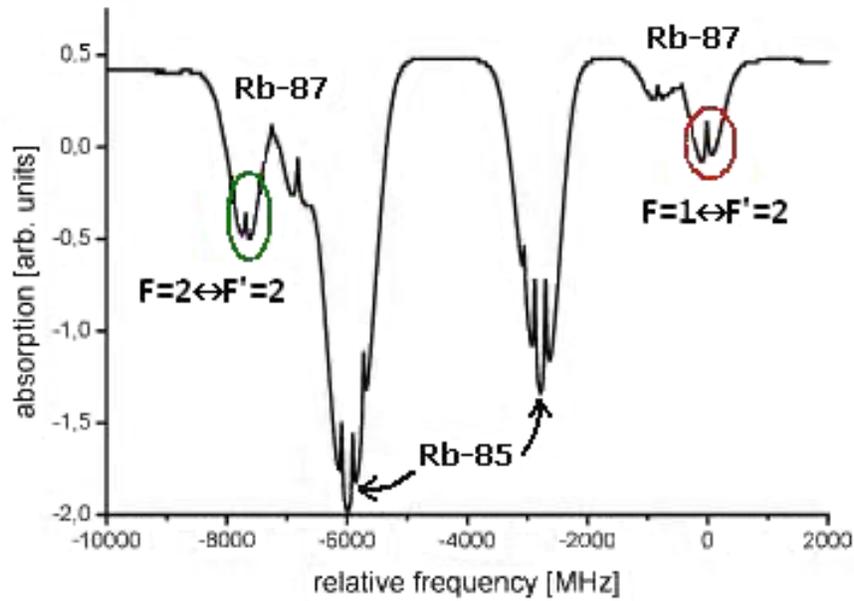
Figure 9: Saturation absorption D1 spectrum of ^{85}Rb and ^{87}Rb. The control laser was tuned to the transition circled in red. The probe laser was tuned to the one circled in green.

All these observations confirmed that this signal truly was the emitted Stokes signal. An image of the Stokes field taken by a simple webcam is shown in Figure 10; as expected, the Stokes signal could be seen when the camera was positioned at an angle of $\approx$ -0.2° with respect to the control field when the angle between the control and probe field was $\approx$ 0.2°.
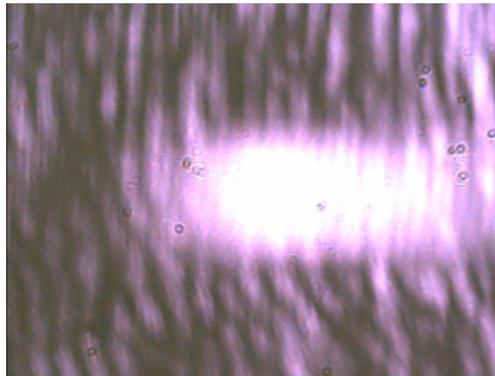
Figure 10: Stokes signal as observed by the webcam.

3.2.2   Optimizing Stokes emission

Figure 11 displays the probe and Stokes signals as observed in the non-colinear setup; the background due to room lighting was subtracted from the signals. In contrast to the symmetric probe and antisymmetric

12
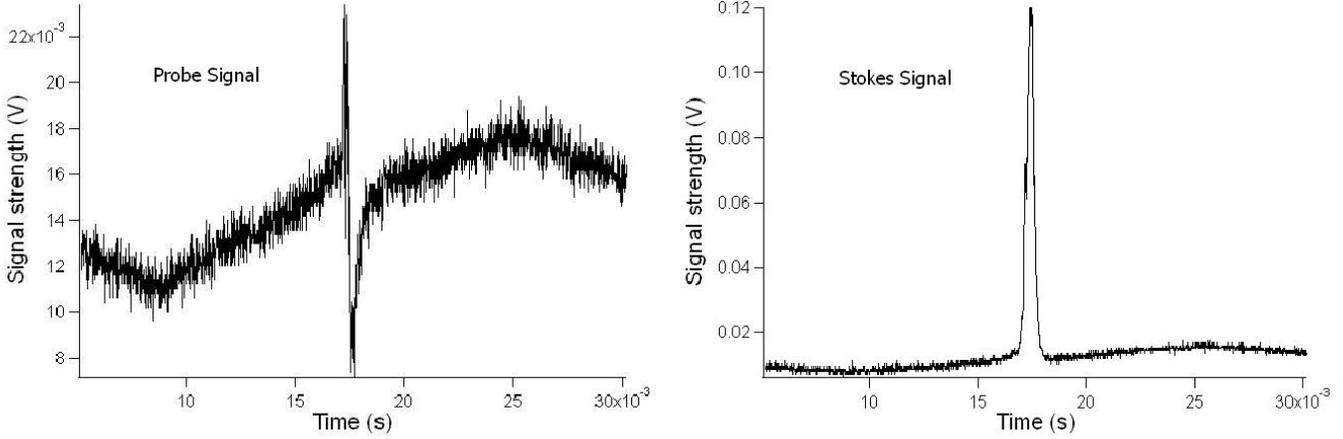
Figure 11: Probe and Stokes signal at detuning = 0.7 GHz, probe power/control power = 0.47. The x-axis is labeled as "Time" in this figure because the oscilloscope shows the signal as a function of time. However, the passage of time actually reflects the scanning of frequencies by the probe beam. The sweep range was adjusted from one data set to another so the width of various resonances should not be compared.

Stokes signals observed with the colinear setup, in the non-colinear setup the probe resonance is antisymmetric while the Stokes resonance is symmetric (as expected since the Stokes is purely being emitted).

To find the optimal conditions for Stokes emission, I measured the Stokes signal at different laser detunings and at different ratios of probe/control power. The frequency detunings of the lasers were measured using a wavemeter to obtain ±0.1 GHz precision and were always to the blue of the ^{87}Rb transition frequencies. The control power was consistently maintained around 4.0 mW while the probe power was varied. I measured the Stokes peak height directly from the data and plotted it as a function of laser detuning and laser power ratios in Figure 12a and Figure 12b. The two plots represent data taken on different days; the two data sets were fairly consistent with one another. The Stokes signal height decreases with decreasing probe/control power ratios; this result is interesting because most literature about FWM recommends a probe/control power ratio two magnitudes smaller than the ones I used. A probe/control power ratio of 0.5 is probably optimal, because even though Stokes signals are even larger for a probe/control power ratio of 0.7, these signals also have a much larger background signal due to more of the probe and control fields leaking through. The optimal laser detuning appears to be between 0.4 GHz and 0.6 GHz; within this range, I observed Stokes signals with peak heights up to 126 mV, corresponding to a 323 nA current. However, the data is not entirely consistent; for example, the Stokes signal shown in Figure 11, which was observed approximately one week before the other measurements, has a 110 mV peak, corresponding to a 282 nA current, at a laser detuning of 0.7 GHz and a probe/control power ratio of 0.47. If one considers the ±0.1 GHz uncertainty in the detuning measurement, then this signal still falls within error of the optimal detuning range of 0.4-0.6

13

GHz; nonetheless, it is almost twice as strong as the signals measured at 0.6 GHz detuning from the following week. The discrepancies between data sets may be due to slight changes in alignment that occurred between one day and another. However, even if the data sets taken on different days are not entirely consistent when it comes to optimal conditions for Stokes emission, it is clear that both the probe/control power ratio and the laser detuning from resonance can significantly impact the strength of the Stokes signal.
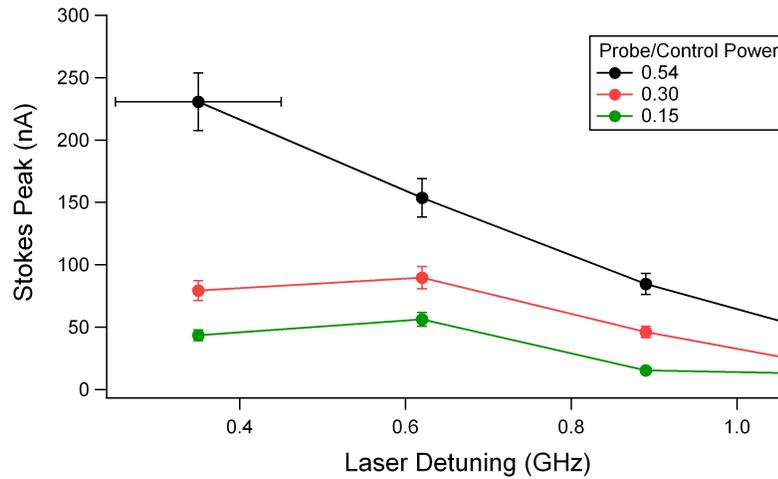
Figure 12a: Stokes peak current vs. laser detuning. The laser detuning measurements all have a ±0.1 GHz statistical uncertainty, shown for one point. The current measurements have a ±10% statistical uncertainty.
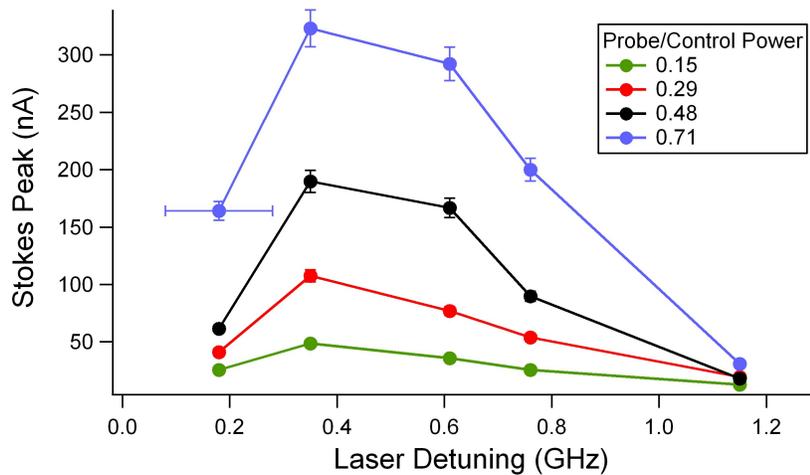
Figure 12b: Stokes peak current vs. laser detuning. The laser detuning measurements all have a ±0.1 GHz statistical uncertainty, shown for one point. The current measurements have a ±5% statistical uncertainty.

3.2.3   Probe and Stokes dependence on optical depth

After the measurements described in section 3.2.2 were taken, the experimental setup was left unused for a month; when I turned on the lasers again to study the dependence of FWM on optical depth, I had to realign many optical elements because the lasers had drifted during this time. After these adjustments, the angle between the control and probe beams was ≈0.4°. Measuring the Stokes signal at different laser detunings, I found that the highest signals now appeared to the red of the F=2→F'=2 transition and to the blue of the F=2→F'=1 transition; in fact optimal Stokes emission occurred at a frequency in the middle of these two transition frequencies, at a detuning of ≈0.4 GHz to the red of the F=2→F'=2 transition. I set the control and probe powers to 5.8 mW and 2.8 mW, respectively, yielding a probe/control power ratio of 0.48; I chose to use higher laser powers than I had previously in order to increase the Stokes signal, which was bound to decrease with decreasing optical depth. Then, the temperature controller for the Rb cell was turned off, and I took measurements of the probe and Stokes signals as the temperature, and thus the optical depth, decreased. The optical depth was lowered all the way to 1.5; the Stokes signal was still observable with the photodiode at this optical depth, although its peak height corresponded to a current of only 3.8 nA and its signal-to-noise ratio was 1.2. The Stokes signal was visible on the webcam only down to an optical depth of 8, at which point the Stokes current was 18 nA.
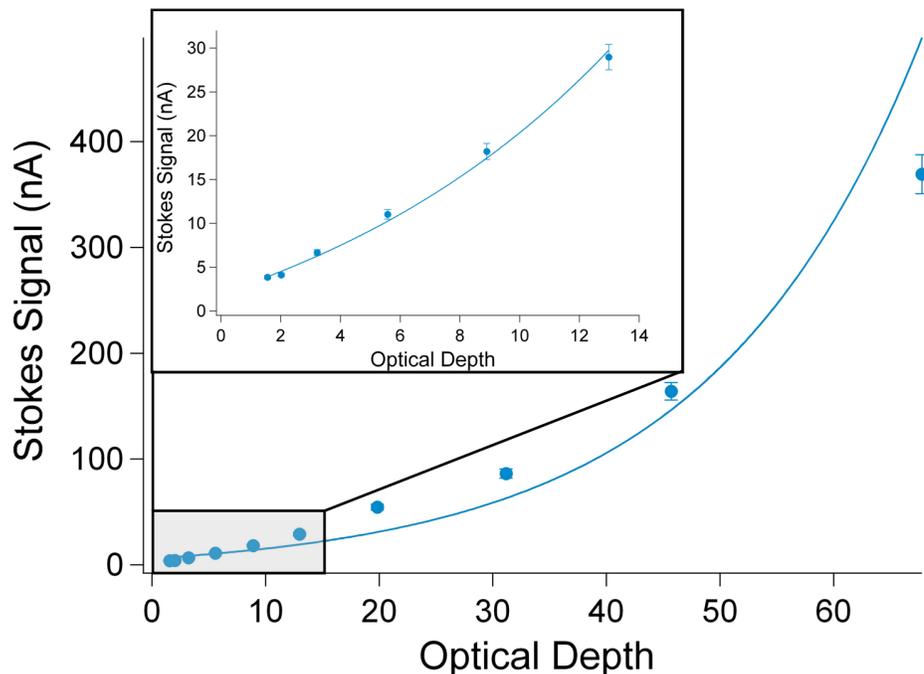
Figure 13: Stokes peak current vs. optical depth. The current measurements have a ±5% statistical uncertainty.

Figure 13 displays the Stokes signal dependence on optical depth, while Figure 14 displays the probe signal dependence on optical depth; in both cases, I measured the height of the resonance peaks in volts and converted it into amps based on the photodiode resistor values. As already seen in the colinear setup, the Stokes signal decreases exponentially with decreasing optical depth. An approximate fit for the Stokes data is:

$$\text{Stokes} = 13e^{0.054 \times OD} - 7 \tag{15}$$

However, as can be seen in the inset of Figure 13, at lower optical depths, the Stokes signal begins to decrease more rapidly, and thus a better fit for the data at optical depths below 13 is:

$$\text{Stokes} = 13e^{0.088 \times OD} - 11 \tag{16}$$

The probe signal does not decrease exponentially as it did in the colinear setup. Instead, for optical depths below 13, the probe signal decreases fairly linearly with decreasing optical depth, as can be seen in the inset of Figure 14, and it increases exponentially with decreasing optical depth for optical depths above 13. In the colinear setup, the probe signal decreased exponentially with decreasing optical depth for optical depths below 14. Thus, in both setups, the probe signal decreases with decreasing optical depth for optical
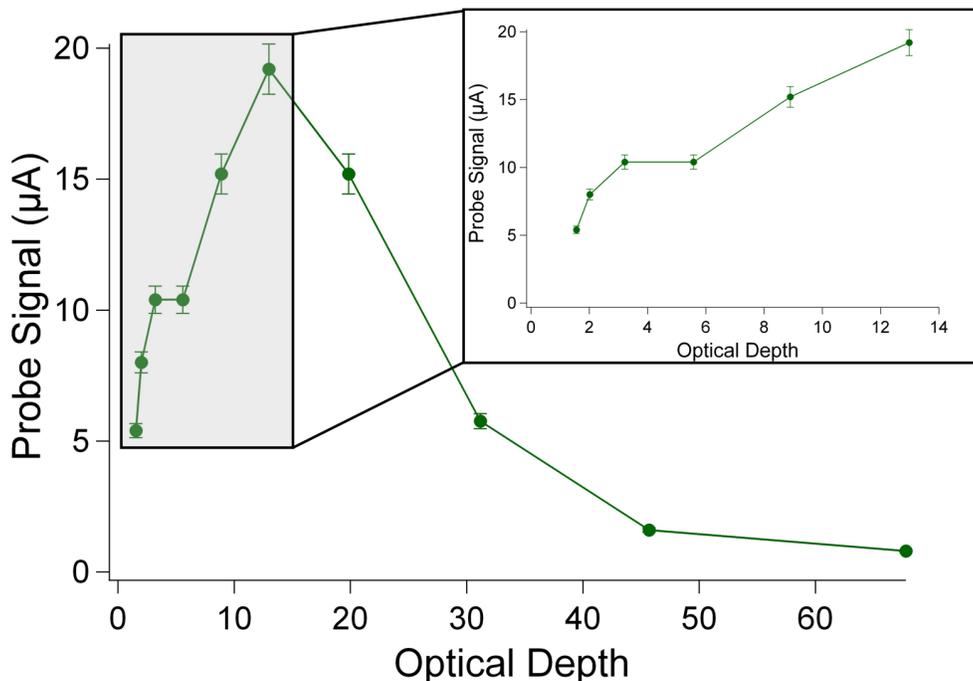
Figure 14: Probe peak current vs. optical depth. The current measurements have a $\pm 5\%$ statistical uncertainty.

depths below 13-14, even though the rate at which it decreases differs. The reason for this difference is unclear, and since these optical depth dependent measurements require a lot of time to take, I did not repeat

16

them, so that it is difficult to determine how significant this difference is. However, the most interesting result of this probe data is that the probe peak is still significant at low optical depths; at an optical depth of 1.5, the probe peak is 5.4 μA. Since this probe FWM signal is large enough to be easily detected, it can be a good indicator of whether FWM is occurring when using cold atoms. Once a FWM signal is observed on the probe, then the weaker Stokes signal can be found and optimized by adjusting the photodiode position and gain, the laser powers and frequency detunings, and the angle between the laser beams.

4 FWM in Cold Atoms

After observing both Stokes and probe FWM signals at low optical depths in the Rb vapor cell, and determining the variables that can optimize Stokes emission, I assembled the non-colinear setup discussed in 3.1 to be tested with cold atoms trapped by Aubin's magneto-optical trap (MOT). Performing this experiment with cold atoms proved to be more complicated and required several adaptations to the experimental setup, but interaction signals were observed which may be the result of FWM.

4.1 Experimental Setup

4.1.1 Magneto-Optical Trap

In ultra-cold atom experiments, the cooling and trapping of atoms with a MOT is often the first step towards producing ultra-cold quantum gases. A MOT has four basic components: an ultra-high vacuum glass cell, a dispenser which provides room temperature atoms to the cell, six intersecting laser beams, and two magnetic quadrupole coils. Figure 15a is a photograph of the MOT apparatus. The vacuum system needs to provide at least a 10^{-9} Torr vacuum. The laser beams are 3 pairs of counter-propagating beams oriented along three different orthogonal axes, as shown in Figure 15b. They cool the room temperature atoms via Doppler cooling to temperatures on the order of 100 μK; for example, they slow down Rubidium atoms to velocities $\approx$10 cm/s, corresponding to a temperature of $\approx$180 μK. The two magnetic coils are set up in an anti-Helmholtz configuration generating a magnetic quadrupole field gradient. This spatially dependent magnetic field changes the energy levels of the atom via the Zeeman effect. The result of the combination of lasers and magnetic coils is that the atoms are pushed towards the midpoint between the two coils where the magnetic field is zero. Thus, the atoms are both cooled and trapped by the MOT.

In this part of the experiment, I tried to observe FWM with atoms cooled to $\approx$100 μK and trapped by the MOT; the ultimate goal is to observe FWM in ultra-cold degenerate atoms and image them.
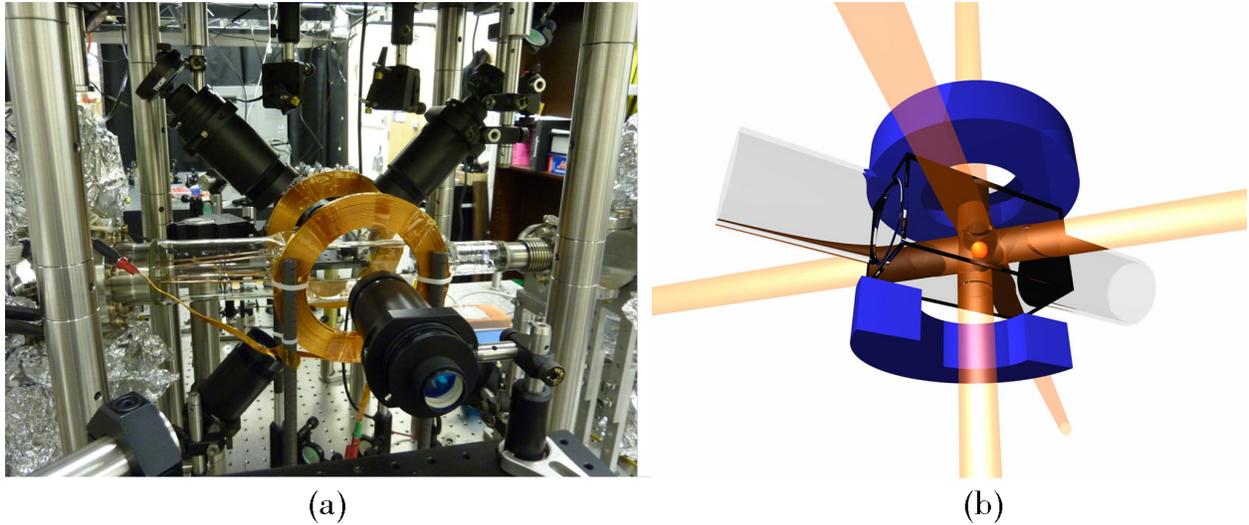
Figure 15: (a) Photo of MOT apparatus. (b) Schematic of MOT apparatus [9]. The orange ball represents the trapped atoms.

4.1.2   D2 line

Whereas Novikova's vapor cell experiments tend to involve the Rb D1 line, Aubin's MOT experiments tend to involve the Rb D2 line. Thus, one important difference of the cold atom setup as opposed to the setups previously discussed is that the two lasers were D2 lasers. A D2 laser similar to the probe D1 laser in the non-colinear setup provided the control beam; this laser could scan over a large frequency range and be tuned to any of the ^{87}Rb resonances. The probe beam came from the same laser source as the MOT beams; therefore, it was locked to the same frequency as the MOT beams, which are 8 MHz below the F=2→F'=3 transition frequency. However, in order for FWM to be possible, the control and the probe needed to be able to access the same excited state from the two different ground states; the F'=3 excited state is only accessible from the F=2 ground state due to selection rules. The F'=1 and the F'=2 excited states are the only ones that are accesible from both the F=1 and F=2 ground states. The F'=2 state was selected since a single AOM could be used to lower the frequency of the probe source laser from the F=2→F'=3 transition to the F=2→F'=2 transition. Figure 16 shows the transitions involved in FWM with the D2 line.

4.1.3   Optics Setup and Beam Alignment

Figure 18a is a photograph of the first stage of the experimental setup. The light from the optical fiber was the probe beam, which propagated through an AOM that decreased its frequency by 261.5 MHz, making the probe detuned by 5.6 MHz to the blue of the F=2→F'=2 transition. The control beam from the D2 laser passed through an anamorphic prism pair and an optical isolator. A small fraction of the light was
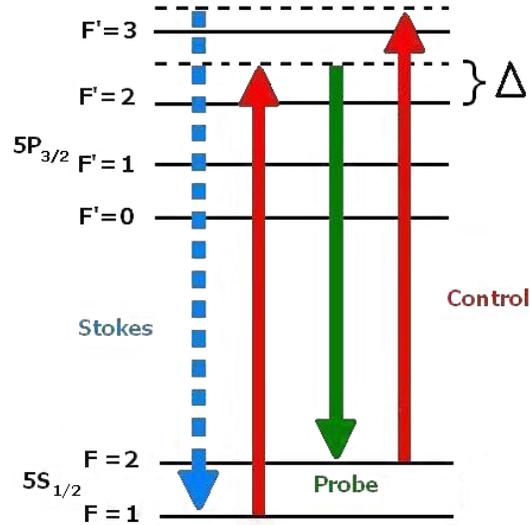
Figure 16: ^{87}Rb D2 line ground and excited states

then picked off by a glass slide and sent through a Rb reference cell; the light was reflected back through the cell by a mirror at the opposite end so that the photodiode could be used to see the saturated absorption D2 spectrum of Rb (shown in Figure 17) which is used to tune the control field to the F=1→F'=2 transition frequency. Both the probe and control passed through a half-wave plate followed by a beamsplitter, ensuring
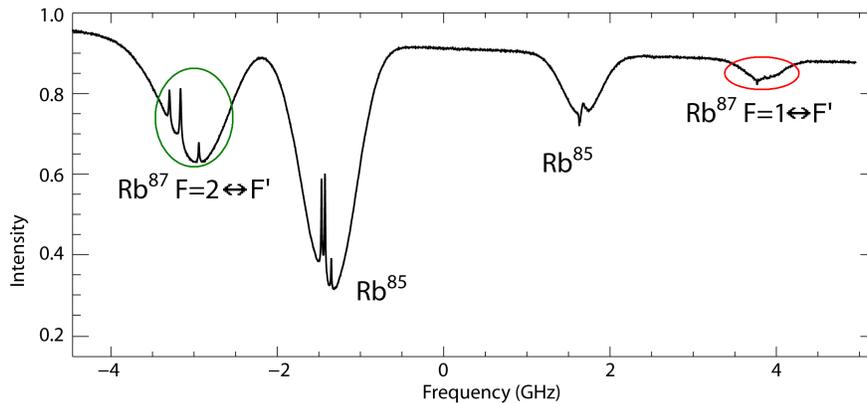
Figure 17: Saturation absorption D2 spectrum of ^{85}Rb and ^{87}Rb (adapted from [10]). The control laser was tuned to the transition circled in red. The probe laser was tuned to the one circled in green.

that each beam was linearly polarized. Adjusting the half-wave plate changed the power of the beam passing through the beamsplitter. As shown in Figure 18b, the control beam passed through an additional half-wave plate which was fixed so that the polarization of the control was orthogonal to that of the probe. Both

19

beams were then sent through the MOT at an angle of $\approx$0.5° relative to one another. The control and probe beams were aligned to the MOT separately; during alignment, the control field was tuned to the F=2→F'=3 transition. One could tell when a beam tuned to an F=2→F' transition was aligned to the MOT because it "killed" the MOT; this additional field excited atoms out of the F=2 state, depopulating this ground state so that the MOT lasers could no longer interact with the atoms and keep them trapped. Finally, Figure 18c shows the polarizing beamsplitter on the other side of the MOT which blocked the control field but allowed the probe and Stokes fields to pass through. Figure 18c also shows the edge mirror which separated the probe and Stokes beams, and the two photodiodes set up to detect the signals (the probe photodiode had a 10 kΩ resistor and the Stokes photodiode had a 390 kΩ resistor).
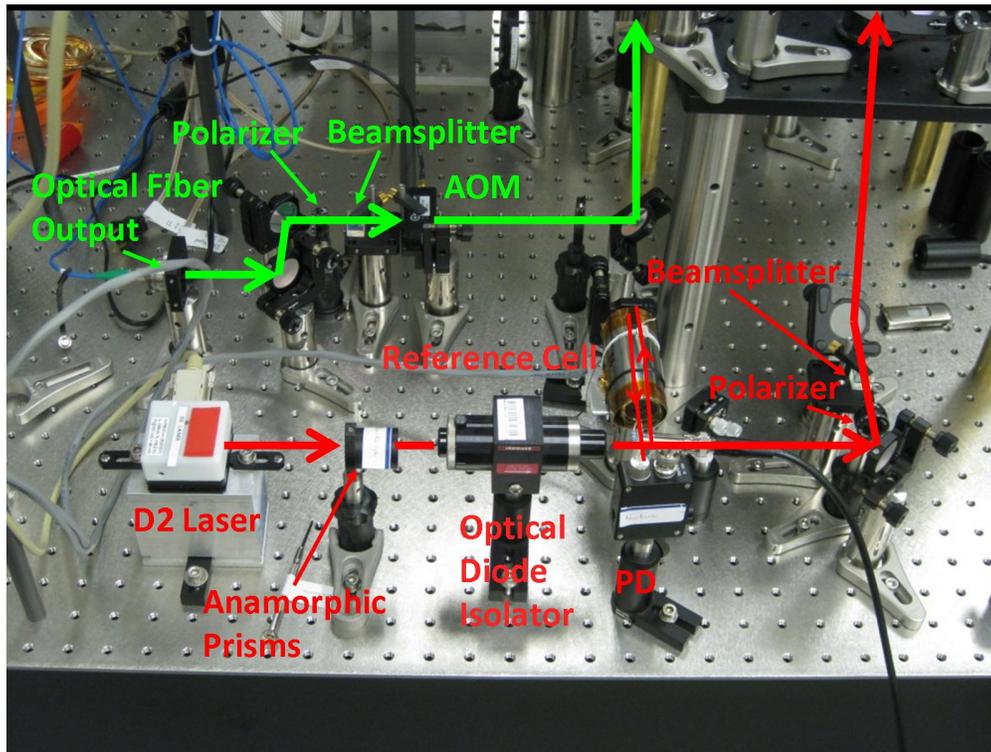
Figure 18a: First stage of setup

4.1.4   Pulsed experiments

The final complication in performing the FWM experiment with cold atoms is that the experiment must be run using pulses. To detect FWM, the probe and the control fields should be the only fields interacting with the atoms. However, when the six MOT lasers and the magnetic coils are off, the atomic cloud expands and falls down due to gravity. Thus, before each experimental run, the six MOT lasers and the magnetic coils had to be on for 5 s to trap a significant number of atoms (on the order of 10^8-10^{10} atoms). The control
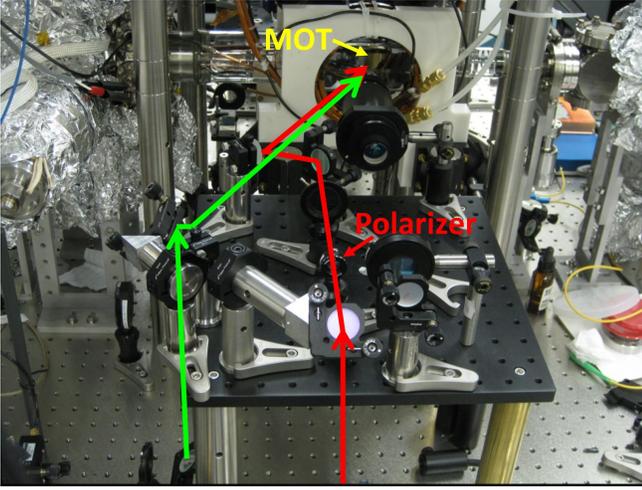
Figure 18b: Second stage of setup
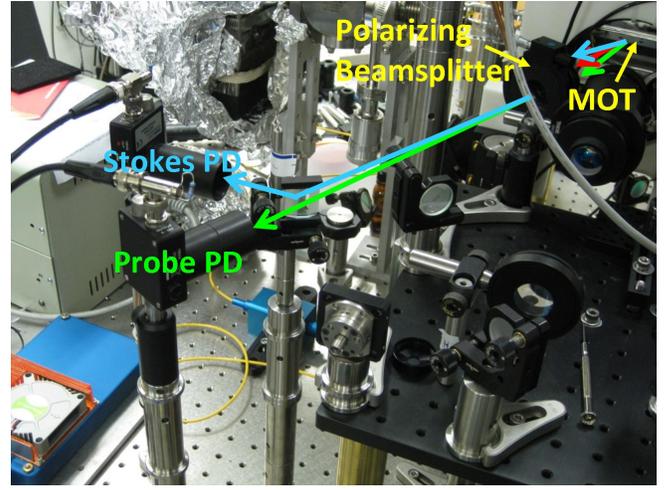
Figure 18c: Third stage of setup

field scanning around the F=1→F'=2 transition was also on at this point, because it helps repopulate the F=2 ground state, which helps the atoms remain trapped. The probe field, however, could not be traveling through the MOT, because it "kills" the MOT. Thus, after the MOT was on for 5 s, it was blocked by a mechanical shutter while the probe field was turned on for 5 ms. Turning the probe field on and off amounted to turning the AOM it passed through on and off; when the AOM was on, a first order diffraction peak appeared which was aligned with the MOT, but when the AOM was off, the beam simply went straight through the AOM and was not aligned with the MOT. After the probe field is allowed to interact with the trapped atoms for 5 ms, the atomic cloud will have expanded and fallen. Thus, the control and probe could interact with the ultra-cold atoms only in 5 ms pulses. Table 1 summarizes the timeline of the pulsed FWM experiment. The fact that the control field completed a frequency scan every 20 ms introduced another complication. During the 5 ms that the control and probe interact with the MOT, only 1/4 of the desired control frequency range is scanned, so that if no FWM signals are detected, it may simply be because the frequency range that was scanned in those 5 ms did not include the resonant frequency for the two-photon process.

Table 1: Timeline of Pulsed Experiment

	5 s	0.2 ms	0.1 ms	5 ms
	MOT traps atoms	Shutter moves in place	Magnetic field turns off	FWM lasers on
MOT lasers	On	Blocked by shutter	Blocked	Blocked
Repumper laser	On	Off	Off	Off
Magnetic coils	On	On	Off	Off
Probe laser	AOM off	AOM off	AOM off	AOM on

4.2 Data and Analysis

4.2.1 Detection of interaction signals

The pulsed FWM experiment was run with a 0.7 mW control field and a 0.25 mW probe field. These laser powers were an order of magnitude lower than in the vapor cell experiments, both because there was a limited amount of probe power available after this beam had passed through an optical fiber and an AOM, and also because more powerful lasers would cause the trapped atoms to escape more quickly. The temperature of the trapped atoms had been measured earlier in the day to be $\approx 115~\mu$K.
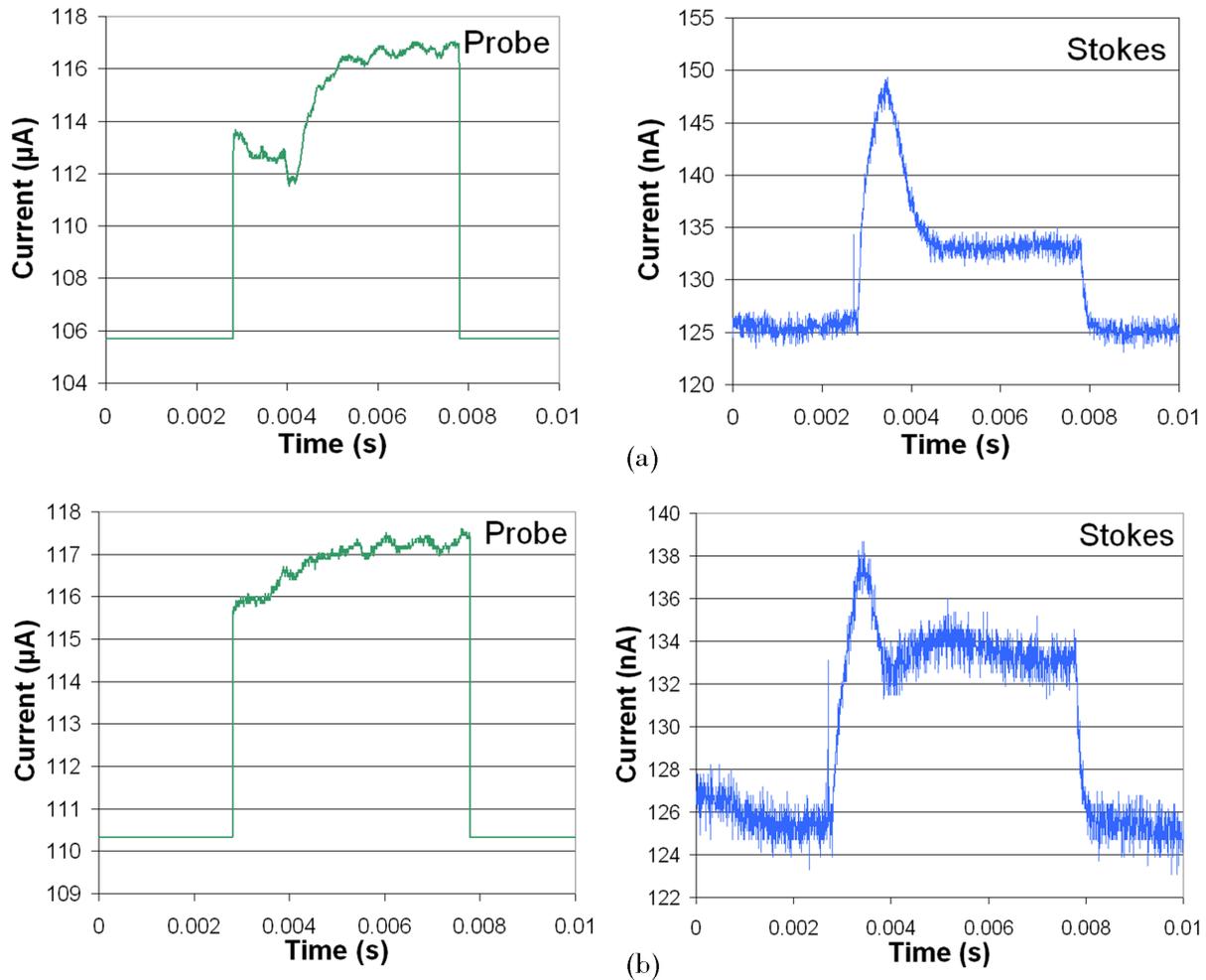
Figure 19: Examples of (a) anti-correlated signals and (b) non-correlated signals.

Both the probe and the Stokes photodiodes detected interaction signals during certain 5 ms pulses; as expected, these signals only appear during some of the 5 ms pulses since the two-photon resonant frequency was only met by some of the 5 ms frequency scans. The signals observed by the Stokes photodiode typically are positive, emission-like peaks, while the signals observed by the probe photodiode are all negative

22

absorption-like troughs. In fact, the majority of the time, the probe and Stokes signals are anti-correlated, meaning that the Stokes has a peak during the same time span that the probe has a trough. Figure 19 provides examples of these signals. These signals are definitely due to the interaction of both the control and probe lasers with the trapped atoms; releasing the trapped atoms or blocking either laser causes the peaks to disappear, as shown in Figure 20. Furthermore, as the control laser is tuned away from the F=1→F'=2 resonance, the peaks diminish significantly in size. Thus, the signals depend on the detuning from the two-photon resonance frequency. This evidence is consistent with the hypothesis that FWM is occuring, although it is not enough to definitively prove it. The highest observed Stokes peak was 7 mV, which corresponds
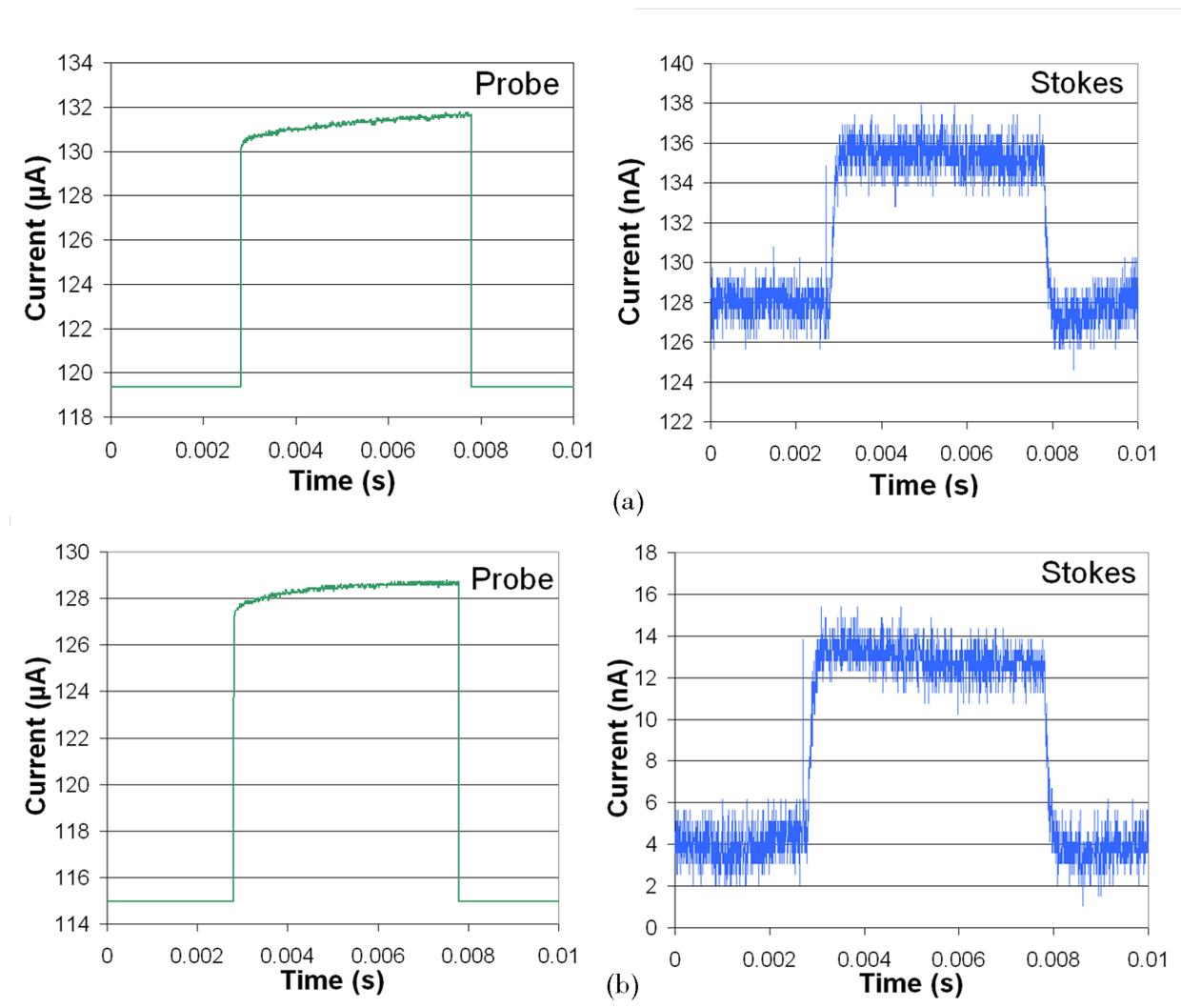
Figure 20: Signals when (a) no atoms are trapped and (b) control field is blocked.

to 18 nA, a signal larger than that expected from the vapor cell experiments (see Figure 21a). The deepest probe trough was 90 mV, corresponding to 9 μA, a signal of approximately the same size as that found in

the vapor cell experiments (see Figure 21b). During some 5 ms pulses, the Stokes photodiode also detects an absorption-like trough rather than a peak; these troughs tend to occur in the middle or towards the end of the pulses. Figure 22 provides examples of this phenomenon, the cause of which is uncertain.
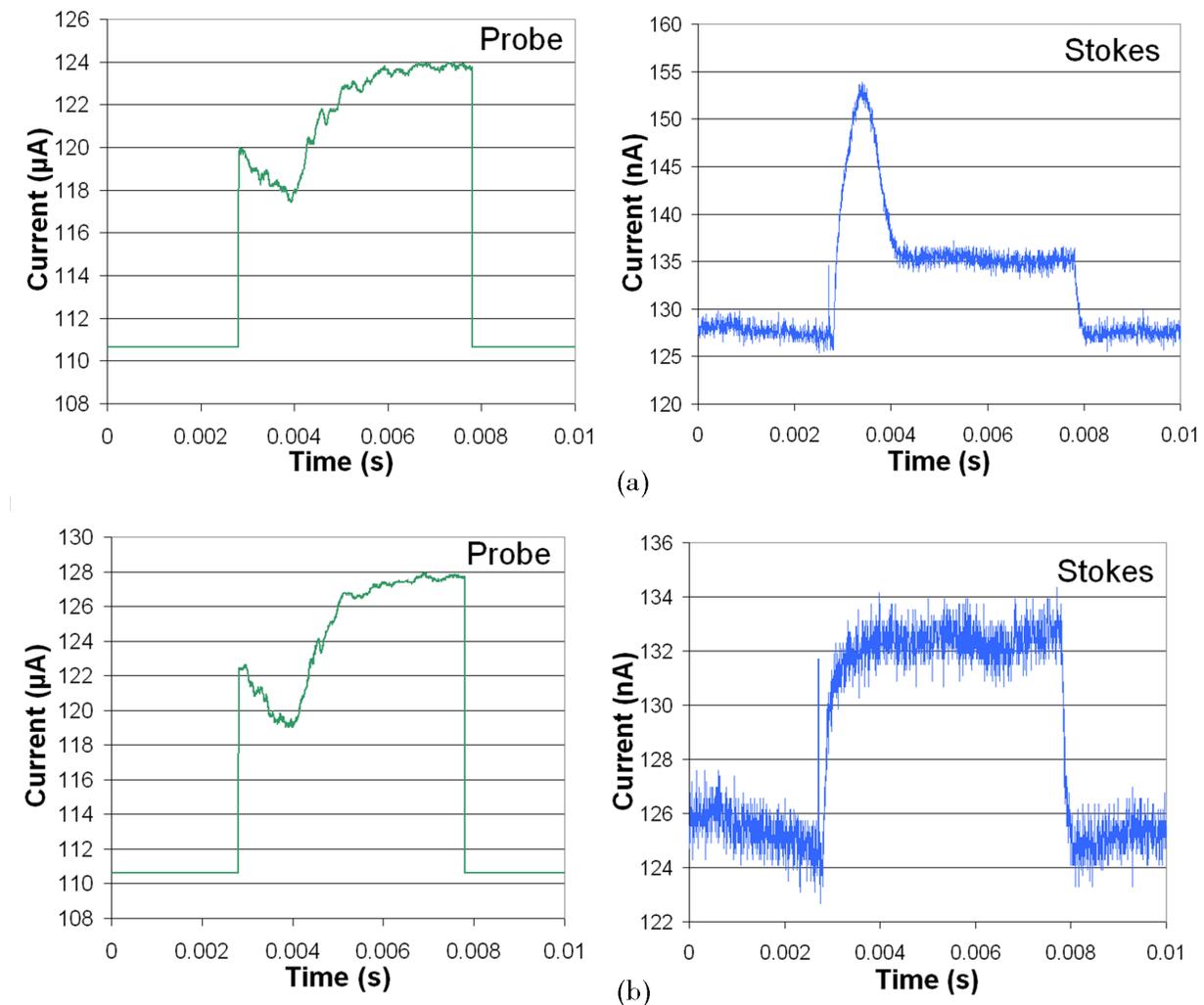
Figure 21: (a) Strongest Stokes peak with corresponding probe signal and (b) strongest probe trough with corresponding Stokes signal.

The Stokes peaks and the probe troughs tend to occur at the beginning of the 5 ms pulses during which the control and probe interact with the atoms. Since more atoms are trapped at the beginning of the 5 ms pulse than towards the end of the pulse, it is possible that a significant peak signal can only be created at the beginning of the pulse when there are more trapped atoms. Another possible explanation for this trend involves the effect of the mechanical shutter which blocks the six MOT beams. When this mechanical shutter clicks into place, it produces small but significant vibrations along the entire optics table; as a result, it causes the probe laser to vibrate at the beginning of each 5 ms experimental pulse. When the probe laser
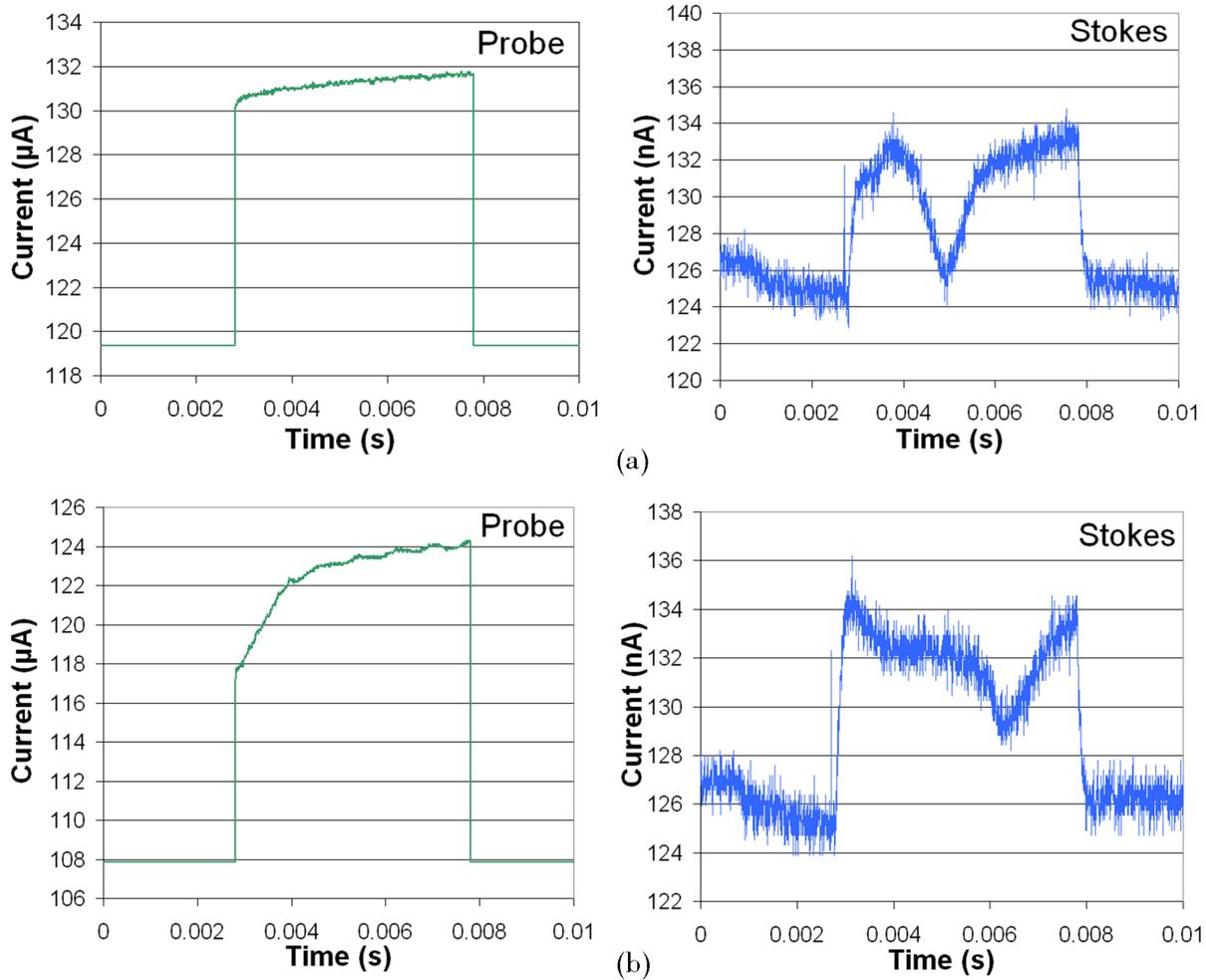
Figure 22: Examples of peculiar absorption-like signals on Stokes and corresponding probe signals

vibrates, it scans over a larger spread of frequencies, making it more likely for the probe and control to be in two-photon resonance during the duration of the shutter vibrations ($\approx$1 ms). Enhancing the shutter vibrations does increase the size of the peaks as well as how often a 5 ms pulse contains a peak or trough at its inception; these effects lend support to the hypothesis that the interaction signals occur at the beginning of the pulse because of the shutter vibrations. It is also worth noting that the width of the peaks and troughs is always approximately 1 ms, independent of how wide a spread of frequencies the control field is scanning over; this lack of correlation suggests that the width of the peaks does not coincide with how much time the two lasers are on-resonance, but rather with a fixed quantity, such as the duration of shutter vibrations or the escape time of the trapped atoms.

4.2.2   Reproducibility of Results

The following day, I hoped to study the interaction signals further but found the results difficult to reproduce. The MOT's position had been changed, so I had to realign the control and probe fields to the MOT, as well as the probe and Stokes photodiodes. Some absorption troughs appeared on the probe, as shown in Figure 23a, but they were not as large as on the previous day. I connected the Stokes photodiode to an amplifier since no signs of interaction could be seen on the Stokes. Changing the laser powers and the frequency detunings did not improve the situation, neither did attempts to adjust the positioning of the photodiodes. However, reducing the shutter vibrations had a positive effect; I started seeing anti-correlated Stokes peaks and probe troughs, as shown in Figure 23b. This result sheds doubt on the hypothesis that
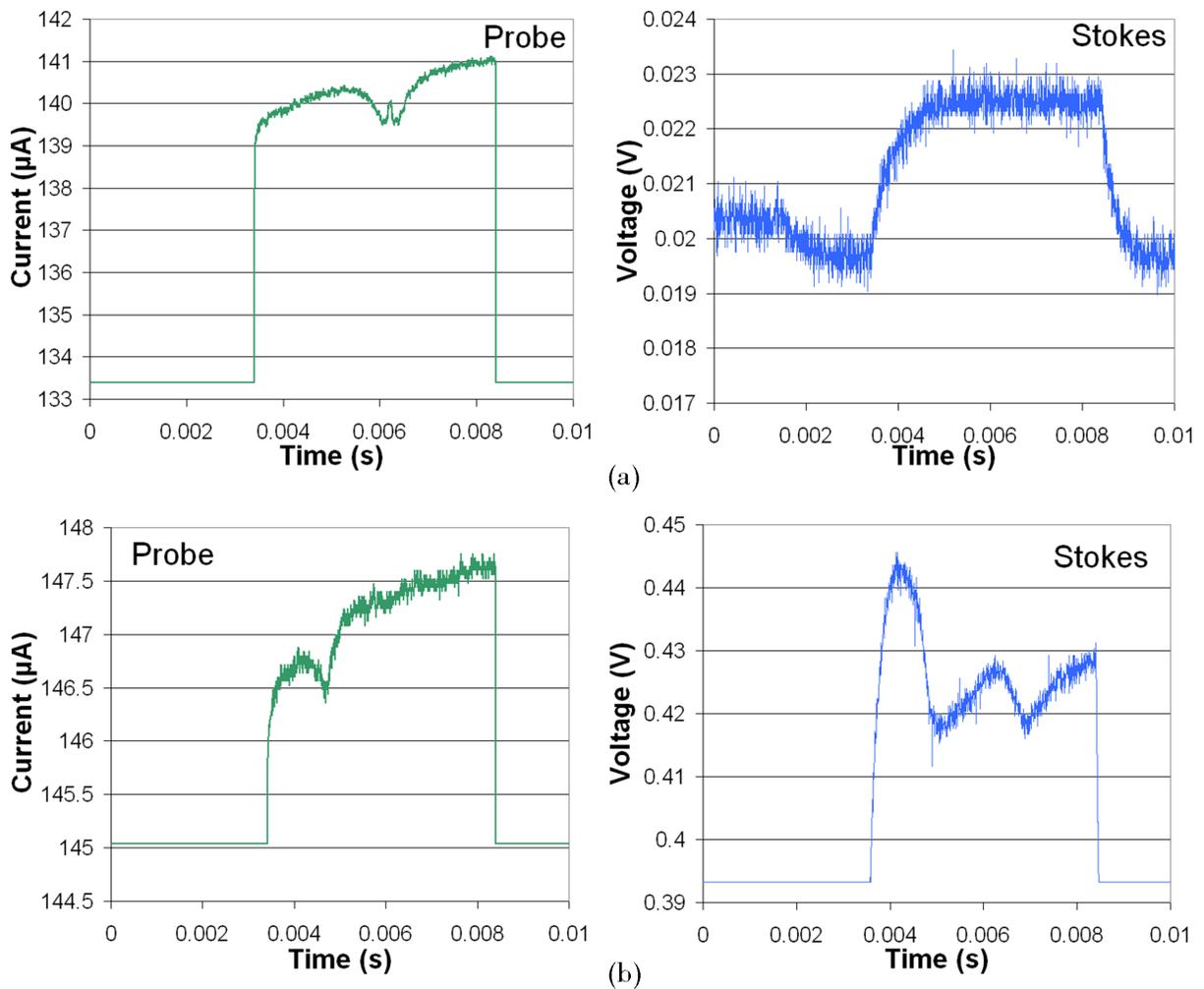
Figure 23: Signals on second day of data-taking: (a) absorption-like features on probe but none on Stokes and (b) emission-like features on Stokes (control power = 0.69 mW, probe power = 0.35 mW)

the shutter vibrations are partly responsible for the interaction signals. Furthermore, the signals were still

much weaker than those from the previous night, possibly because of the MOT itself; on the first data-taking day, the cloud of trapped atoms contained more atoms and displayed more high density regions than on the second data-taking day. Considering how many variables are present in this experiment, it is already a very encouraging sign to have observed any signs of interaction and to have found the same pattern of Stokes peaks and probe troughs in two sets of data. This partial reproducibility is encouraging enough to motivate further study of FWM in cold atoms.

5   Conclusions

Four-wave mixing has been observed in a ^{87}Rb vapor cell in two different configurations, the colinear configuration in which the control, probe, and Stokes fields are all aligned, and the non-colinear configuration in which the control and probe fields enter the cell at a small angle with respect to one another. In both configurations, it was found that the Stokes signal decreases exponentially with decreasing optical depth. At an optical depth of 1.5, the Stokes is a 3.8 nA current signal which is still observable with a photodiode; this suggests that since ultra-cold atoms have an optical depth of ≈ 1, the Stokes photons emitted by these atoms should be detectable. The FWM peak on the probe corresponds to a much higher current of 54 μA at an optical depth of 1.5, and thus it can be used as a more easily observable confirmation that FWM is occurring in low optical depth systems.

A signal consistent with FWM has been observed in cold atoms at a temperature of ≈ 115 μK. Absorption-like features were observed on the probe signal, which were often anti-correlated with emission-like features detected by the Stokes photodiode, which was placed at the expected angle of emission of the Stokes photons. The largest Stokes signal was 18 nA, while the largest probe signal was 9 μA. The features seen on the probe and Stokes depend on the interaction of both the control and probe fields with the trapped atoms; furthermore, the strength of these features depends on the frequency difference between the probe and control fields. These correlations support the hypothesis that these features are due to a FWM interaction. However, they are still not fully understood; the features tend to only appear at the beginning of the 5 ms pulse during which both the control and probe fields are allowed to interact with the trapped atoms, and sometimes the Stokes also shows absorption-like features. These results were reproduced with difficulty and only partially; the features were much weaker during the second round of data-taking. Since this experiment has so many variables, it is difficult to pinpoint the source of this discrepancy, although the most likely problem was that the number and density of atoms trapped by the MOT were lower on the second day.

This study has also determined that Stokes emission significantly depends on both the laser frequency detuning from resonance transitions as well as the absolute and relative powers of the control and probe fields. In the non-colinear configuration of the vapor cell experiment, the optimal conditions for Stokes

emission were a 0.4-0.6 GHz detuning from resonance and a probe/control power ratio of about 0.5 with the control power being 4-6 mW. It was not yet possible to determine these optimal conditions in the case of cold atoms; however, interaction signals were observed with a control power of 0.69 mW and a probe power of 0.25 mW, yielding a 0.35 power ratio.

Although it is still unknown whether an imaging system for cold atoms using the FWM process would be more effective than other current imaging techniques, these results indicate that it is worthwhile to investigate this possibility further, since FWM does seem to occur and be detectable in cold atoms. Further studies of the interaction features seen on the probe and Stokes fields in the cold atom experiment need to be carried out in order to determine more definitively if FWM is happening, how these features depend on different parameters of the experiment, and how they may be related to the number and spatial density distribution of the atoms. Being able to lock both the control and probe lasers would help these experiments run more smoothly as well as provide a means of studying the interaction features as a function of laser detunings from resonance transitions. Once the nA-strength features on the Stokes can be more easily reproduced, an imaging system with a camera should be set up to observe this signal. The photodiode observations can provide temporal information while a camera would provide spatial information about the signal; clearly, this would also be a crucial step in developing an imaging system based on the FWM process. Once a working imaging system is developed for cold atoms, it can then be adapted for use with ultra-cold atoms.

References

[1] P.D. Lett, et al., Powerpoint presentation (2007).

[2] V. Boyer, C.F. McCormick, E. Arimondo, and P.D. Lett, Physical Review Letters 99, 143601 (2007).

[3] C.F. McCormick, A.M. Marino, V. Boyer, and P.D. Lett, Phyical Review A 78, 043816 (2008).

[4] V. Boyer, A.M. Marino, and P.D. Lett, Physical Review Letters 100, 143601 (2008).

[5] P.R. Berman, and Xiaodong Xu, Physical Review A 78, 053407 (2008).

[6] "FM Saturation Spectroscopy." http://www.footballphysics.utk.edu/optics507/modules/m10/saturation.htm. Modified April 13, 2008. Accessed May 1, 2010.

[7] N. B. Phillips, A. V. Gorshkov, and I. Novikova, J. Mod. Opt. 56, 1916 (2009).

[8] R.C. Pooser, A.M. Marino, V. Boyer, K.M. Jones, and P.D. Lett, Optics Express Vol. 19, No. 19, 16722 (2009).

[9] "Ultra-cold Matter Research: Apparatus for Ultra-cold Matter."
http://saaubi.people.wm.edu/ResearchGroup/Research/UltraCold_Research/Apparatus_UltraCold/
Apparatus_UltraCold.html. Modified January 17, 2007. Accessed May 1, 2010.

[10] "MOGlabs Diode Laser Elecronics." http://www.moglabs.com/. Modified March 12, 2010. Accessed
May 1, 2010.